Journal of Materials Chemistry A

ROYAL SOCIETY OF CHEMISTRY

PAPER

View Article Online
View Journal | View Issue

Cite this: J. Mater. Chem. A, 2025, 13, 35470

Recyclable layered chromite-based porous film for water cleaning†

Royston Mathias, Raksha D. Salian and Partha Kumbhakar *

Received 3rd March 2025
Accepted 11th July 2025

DOI: 10.1039/d5ta01758k

rsc.li/materials-a

The oil spillage and pollutants in water bodies are a significant concern in the present time. To address this concern, a porous and superhydrophobic nanocomposite film containing layered natural chromite ores with a polymer was fabricated using a simple solution casting method. The flexible film exhibited a good tensile strength of 1.022 kg mm^{-2} and self-cleaning properties. It showed an excellent oil adsorption of up to ~268% for castor oil and an adsorption efficiency of ~90% for toxic cationic dyes. The presence of high surface charges on the chromite nanosheets enhanced its adsorbing capability. Furthermore, even after being resynthesized from old used film, the composite film maintained its mechanical strength, hydrophobicity, and adsorbing capabilities. Therefore, we believe that the present work can help in cleaning oil and other pollutants from large water bodies and consequently preserving aquatic life.

1 Introduction

Currently, water pollution from oil spillage and organic contamination in oceans is a major challenge in the preservation of aquatic life.[1] Oily wastewater and toxic dye-containing wastewater often coexist owing to daily life activities, such as industrial practices, marine transportation, engine failures, and other manufacturing processes, thereby posing a hazard to mainly aquatic life, human health, and the ecosystem.[2–4] Different technologies have been employed to overcome these issues; however, they could not be sustained for long because of their low efficiency and stability.[5–7] Therefore, there is a crucial need to develop cutting-edge techniques and extraordinary materials for the separation of pollutants from water. Several traditional methods, including membrane separation, gravity separation, and membrane filtration, have been developed for these purposes.[8]

Generally, oil separation from oil–water mixtures relies on gravity-driven filtration methods.[9] However, because oil has a lower density than water, this approach presents certain challenges when removing oil from large water bodies. Therefore, adsorption techniques using porous media, gel-based membranes, and porous materials, such as sponges, are employed to remove oils and other contaminants from the water surface through adsorption. One of these techniques is oil adsorption using nanocomposite films. This technique mainly depends on the hydrophobicity of the film. Therefore, superhydrophobic and superoleophilic materials are at the centre of attention for these applications and extensive research is ongoing to increase the efficiency of oil–water separation and dye adsorption using this method.[10–19] Superhydrophobic surfaces with high contact angles have the potential to achieve exceptional water-repelling qualities.[20] The contact angle of water on these surfaces is also affected by the chemical and structural factors of the composite materials.[21,22] In the recent years, several nanoparticles, including SiO_2, TiO_2, and ZnO, have been combined with polymers to alter the surface wettability of polymer-based sponges, fabrics, and porous metal meshes.[23–28]

Previous literature on oil/water separation has shown that the wetting properties of membranes can be enhanced by synthesizing advanced two-dimensional (2D) polymer composites.[29–34] Nanoparticle-based composites have been synthesized using a variety of techniques, including solution casting,[35] melt mixing,[36] dip coating,[37] spray coating,[38] sol–gel,[39] chemical vapor deposition,[40] electrospray,[41] and layer-by-layer synthesis.[42] However, owing to their poor separation efficiency, there remains a critical need to develop novel functional materials and advanced interfaces with excellent selectivity and high separation efficiency for separating oil–water mixtures. Also, the recyclability of these composites is crucial, and there is a dire need to recycle these nanocomposites, as discarding damaged films will increase pollution and in turn affect aquatic life and fill the land with polymer waste. Major research has already been reported on oil cleaning using nanocomposites; however, there are very limited reports on the recycling of composites.

In this work, we used the solution casting method to synthesize a porous polymer-2D material composite film, in which the polymer serves as the matrix and the atomically thin natural ores (chromite nanosheets) are used to enhance the

Department of Physics and Electronics, Christ University, Bangalore 560029, India. E-mail: partha.kumbhakar@christuniversity.in

† Electronic supplementary information (ESI) available. See DOI: https://doi.org/10.1039/d5ta01758k

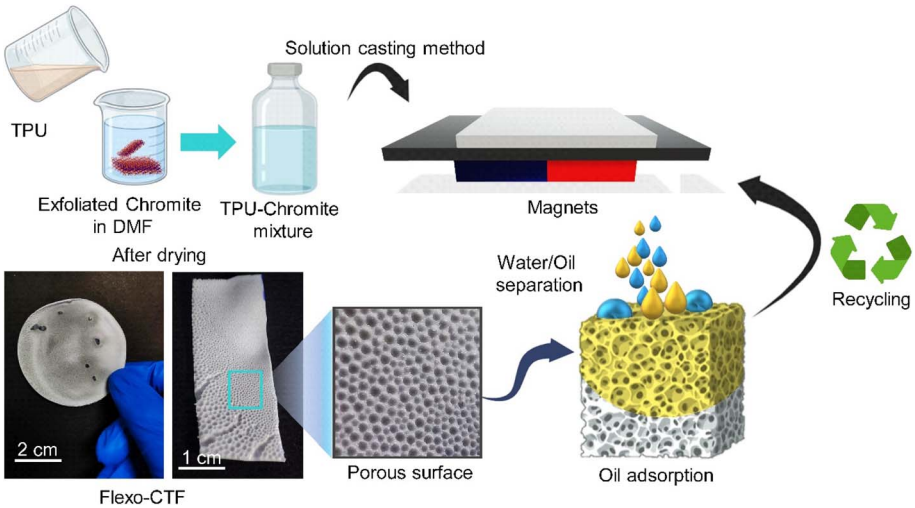

Fig. 1 Schematic of the synthesis of Flexo-CTF using the solution casting method, porosity of the synthesized material and the separation of oil from water.

separation properties (Fig. 1). The wettability, oil adsorption property and toxic dye adsorption of the film were investigated. The dispersed nanosheets in the matrix were used to enhance the properties of the composite. The highly flexible 2D chromite-TPU composite film (Flexo-CTF) demonstrated a superhydrophobic and oleophilic surface with a remarkable oil adsorption capacity of up to ~268% for castor oil. The microscopic techniques were used to study the morphological properties of 2D chromite and Flexo-CTF. Additionally, this Flexo-CTF is reusable and recyclable. The pollutants or adsorbed oil can be cleaned after prolonged use and further employed to clean water bodies. Furthermore, as the film becomes damaged due to extensive use, it can be recycled through simple chemical and thermal treatments and can continue to be used for oil cleaning in water bodies. The Flexo-CTF is also easy to manufacture and scalable due to its low energy consumption during fabrication. The film can be utilized in oceans where oil spills occur to collect all the oil without contaminating the water further, thereby providing a safe and healthy environment for aquatic life. This film avoids the need for gravity-driven techniques as the oil is adsorbed onto the film surface. Therefore, the current approach enables Flexo-CTF to be used for a longer period, making it a sustainable and environmentally friendly solution.

2 Experimental section

2.1 Materials

Thermoplastic polyurethane (TPU) was obtained from Sigma-Aldrich, Bangalore, India. Chromite ($FeCr_2O_4$) ore was obtained from a local vendor who retrieved it from a chromite mine, Orissa, India. Dimethyl formamide (DMF) of 99.8% purity was obtained from Sigma-Aldrich, Bangalore, India. Acetone of 99.5% purity was obtained from Sigma-Aldrich, Bangalore, India. Castor oil, vegetable oil, red oil, petrol, and diesel were obtained from the local vendors in Bangalore, India. Super magnets with a magnetic field of 4 mT were obtained from Sigma-Aldrich, Bangalore, India.

2.2 The synthesis of 2D chromite

The synthesis of 2D chromite involved crushing the crystal bulk chromite to easily disperse it in the solvent.[43] Here, we used DMF as the solvent because of its ability to disperse the chromite particles effectively. The sample-to-solvent ratio was kept at 1 mg : 5 ml to ensure optimal dispersion. Furthermore, this sample was exfoliated for 2 hours in a probe-sonicator (model: Labman Scientific Instruments). The temperature of the system was controlled using an ice bath. The exfoliation was carried out at room temperature utilizing the Liquid Phase Exfoliation (LPE) method. LPE is an exfoliation method where the vibration in the liquid is transferred to the bulk particles, breaking the weak van der Waals interactions between the layers of the chromite particles to provide thin sheets of chromite. The exfoliated solution was rested for 24 hours to ensure that the larger particles, which were not completely exfoliated, settled to the bottom due to gravity, yielding well-exfoliated and uniformly dispersed chromite nanosheets at the top. This exfoliated solution was further used for various characterizations and applications.

2.3 Fabrication of the flexible TPU composite thin porous film

The fabrication of the Flexo-CTF was performed by a carefully controlled process involving the application of heat and a magnetic field (Fig. 1). The procedure began by setting up a magnetic field using permanent magnets on which a Petri-dish was placed. 100 mg of solid TPU was placed in the Petri-dish, and the exfoliated chromite-DMF solution was gradually added dropwise onto the TPU while the mixture was exposed to a magnetic field, which was applied to influence the alignment and distribution of the chromite particles within the TPU matrix. The solid TPU was dissolved in the chromite–DMF

solution. Simultaneously, the temperature of the system was elevated to approximately ~70 °C. This temperature was chosen to facilitate the uniform dissolution of TPU into the chromite-DMF solution and to form bubbles, which will subsequently form the porous surface. As the temperature increased, more bubbles were formed, resulting in a greater number of pores per unit area. Once complete dissolution was achieved, the temperature was gradually reduced to room temperature to initiate the solidification process. The solution was then allowed to dry under ambient conditions for a period of 8 to 12 hours. During this time, the solvent (DMF) gradually evaporated, leaving behind a solidified porous film consisting of TPU embedded with chromite sheets. The resulting film was referred to as Flexo-CTF.

2.4 Characterization

A scanning electron microscope (SEM) (ThermoFisher (Apreo S LoVac)) attached to an energy dispersive spectrometer (EDS) was used to confirm the morphology of the sample. To confirm the different phases present in the sample, X-ray diffraction (Miniflex 600 Rigaku XRD) was performed. To analyse the structural property of the sample at an atomic level, high-resolution transmission electron microscopy (HRTEM) (Talos F200 G2) was used. Fourier transform infrared spectroscopy (FTIR) was used to analyze the chemical properties of Flexo-CTF. Zeta potential measurements (Malvern Zetasizer nano) were performed to determine the surface potential of the 2D chromite sheets. X-ray photoelectron spectroscopy (XPS) (Thermofisher k-alpha) was performed to determine the surface properties and oxidation states of the synthesized nanocomposite.

2.5 Wettability test for Flexo-CTF

The wettability (hydrophobicity and oleophilicity) of Flexo-CTF was evaluated by observing a drop of oil and water on the film. A drop of pure water was placed on the film while it was horizontally positioned, and the behaviour of the water drop was observed by capturing a video of the drop on the film for 300 seconds. Similarly, the behaviour of a mustard oil drop was observed by capturing a video of the drop on the film for the same time. In both cases, the contact angle of the drops was continuously measured. Further, the Laplace equation is used to measure the oil adsorbing capability of Flexo-CTF, which is given by[44]

$$\Delta P = \frac{\gamma_L \times \cos\ \theta}{R_p} \quad (1)$$

where ΔP is the intrusion pressure. γ_L is the surface tension of the liquid. θ is the contact angle made by the liquid on the surface of Flexo-CTF. R_p is the average pore size on the porous Flexo-CTF.

2.6 Measurement of the dye-adsorption efficiency of Flexo-CTF

A solution of Methylene blue (MB) and Rhodamine B (RhB) dyes at a concentration of 50 mg L^{-1} was prepared in two beakers, and the CTF film was dipped in the solution. The absorption of the dye was observed after 4 minutes, 10 minutes and 24 hours of dipping the film in the solution. The absorbance was calculated using the calorimetric absorbance formula[45]

$$A = -\frac{1}{\beta} \times \log\ \left(\frac{I_{RGB}}{I_{BG}}\right) \quad (2)$$

where $\beta = 0.5$, I_{RGB} is the mean value of the RGB values of the sample and I_{BG} is the mean value of the RGB values of the background. The RGB values were determined by analyzing the image using the ImageJ software. The image of the dye solutions was obtained using a smartphone camera.

2.7 Oil adsorption from water using Flexo-CTF

Different oils, such as mustard oil, red oil, castor oil, petrol and diesel, were used to study the oil–water separation property of the film. 300 mg of each oil was taken in 100 ml of water. The film was dipped in this oil-in-water suspension for 300 seconds, allowing the oil to adsorb on the surface of the film. From this experiment, the adsorption efficiency of Flexo-CTF for different oil suspensions in water was determined.

3 Results and discussions

3.1 Structural and morphological properties of Flexo-CTF

The structural and morphological properties of the film were analyzed using optical and scanning electron microscopy (SEM) images. The optical image of the porous film is displayed in Fig. 2a. It shows the presence of porosity in the film. Fig. 2b shows the SEM image of the film (top view) and the presence of $FeCr_2O_4$ sheets in the polymer matrix. Using the ImageJ software, the optical image of the film was analyzed, and a 3D plot of the film was generated to visualize the size and shape of the pores (Fig. S1a†). The pores had an average diameter of ~0.02 ± 0.002 cm (Fig. S1b†). The 3D plot of the surface reveals a porous structure with good interconnectivity and the presence of micropores in the film. Further, the SEM image of the film surface provides a clearer view of the porosity of the film, showing that the pores are distributed throughout the film and not only on the film surface (Fig. S2†). All three major elements, Fe, Cr, and O, as well as the elemental variation following exfoliation, are confirmed by the EDX spectra (inset of Fig. 2b). The crystalline peaks in the XRD pattern of the exfoliated sample, displayed in Fig. S3,† closely matched those of the spinel phase of $FeCr_2O_4$ [no: mp-1104680]. The TEM image of the exfoliated chromite is shown in Fig. 2c, and it is evident that thin sheets were formed. We present the high-resolution TEM (HRTEM) image (Fig. 2d) of the sheets and demonstrate the presence of multiple layers of atomically thin chromite. The presence of lattice defects was also studied using the fast Fourier transform (FFT) pattern of the image, which shows that the atomic arrangement is not uniform. The edges of the exfoliated sheets showed many surface defects. If the sonication energy exceeds the threshold of the binding energy of the nanosheets, some atoms will be expelled from their lattice during exfoliation. As a result, surface defects are introduced onto the surface of the material. The molecular bonding was

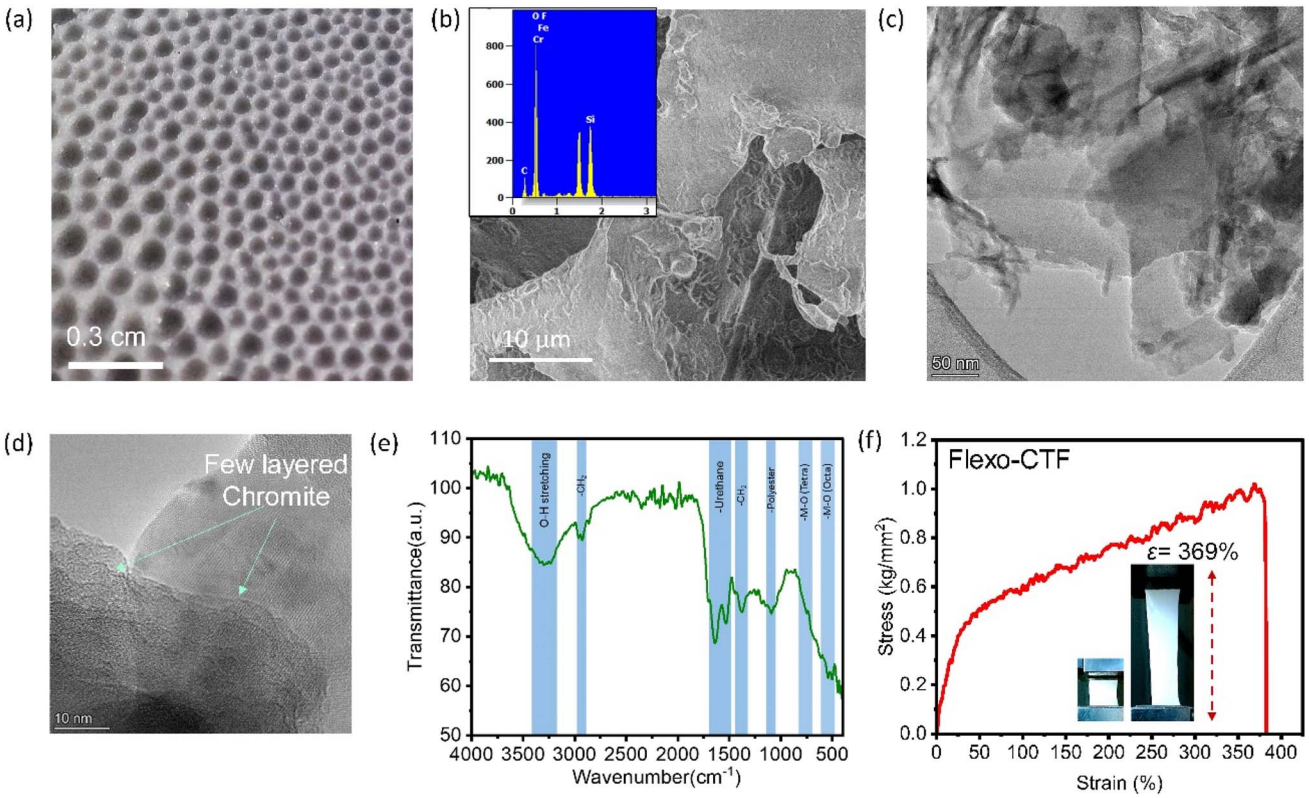

Fig. 2 (a) Optical image of Flexo-CTF showing its porosity. (b and c) SEM image of the chromite nanosheet sample. Inset of (b) shows the EDX spectra of the chromite sample. (d) HRTEM image of the chromite nanosheet. (e) FTIR curve of the chromite nanosheets. (f) Stress–strain curve of Flexo-CTF. Inset of (f) shows the optical image of stretching of the Flexo-CTF film.

further studied using FTIR, which reveals each functional group in the film, as shown in Fig. 2e. The FTIR spectra were examined in the 500–4000 cm^{-1} range. The O–H stretching functional group is represented by the peaks at a wavenumber of about 3302 cm^{-1}.[46] However, at a wavenumber of about 1642 cm^{-1}, the OH bending functional group is observed.[47,48] Additionally, the C–H bending functional group is represented by peaks at wavenumbers of ~2926 cm^{-1} and ~1379 cm^{-1}.[49,50] Tetrahedral and octahedral oxygen–metal M–O bonds are observed in the spectra with transmission peaks at around 748 cm^{-1} and 548 cm^{-1}.[51] This indicates that the divalent and trivalent Fe and Cr ions have occupied the tetrahedral and octahedral positions in the sample, and this range displays the features of atomic vibrations in these positions within the cubic structure.[52] The peaks at 1642 cm^{-1} and 1535 cm^{-1} correspond to the urethane group, and the band at 1094 cm^{-1} corresponds to the polyester group, originating from the TPU in the film.

3.2 Mechanical property analysis of Flexo-CTF

The stress–strain curve of Flexo-CTF is shown in Fig. 2f. The dimensions of CTF used for testing were 17 mm × 10 mm × 0.3 mm ($l \times b \times h$). The CTF was accurately stretched out by mounting the film on a universal tensile testing machine. The rate of elongation was maintained at 5 mm per minute for uniform and gradual elongation. It showed an increasing strain with the increasing applied stress. The maximum elongation showed by the film was ~369% of its original length (inset of Fig. 2f), and it further elongated and broke down at ~382% of its initial length. The load at breakdown was 3 kg F. The tensile strength of the film at peak elongation was measured to be 1.022 kg mm^{-2}. These results show that Flexo-CTF possesses remarkable tensile strength and resistance to external stress. This excellent tensile strength is attributed to the presence of 2D chromite particles in the TPU matrix. These 2D sheets act as effective nanofillers. These 2D chromite particles enhance the structural integrity of the TPU matrix by forming a network of chromite that interconnects the polymer chains. When an external stress is applied, this network of 2D sheets helps distribute the force evenly throughout the film, preventing local stress concentrations and thereby enhancing the tensile properties of the material.

3.3 Wettability for Flexo-CTF

The surface wettability of the CTF film was further studied to determine its efficiency in adsorbing and separating oil from water. The experiment was conducted to analyze the wettability and the contact angle for different liquids on Flexo-CTF. Water and oil were used as the liquids for this experiment, and the behaviour of the drop with respect to contact angle over time was observed for 300 seconds (Fig. 3a). A plot of contact angle *versus* time is shown in Fig. 3b. It was observed that the contact angle of the water in air on the film changed from ~140° to

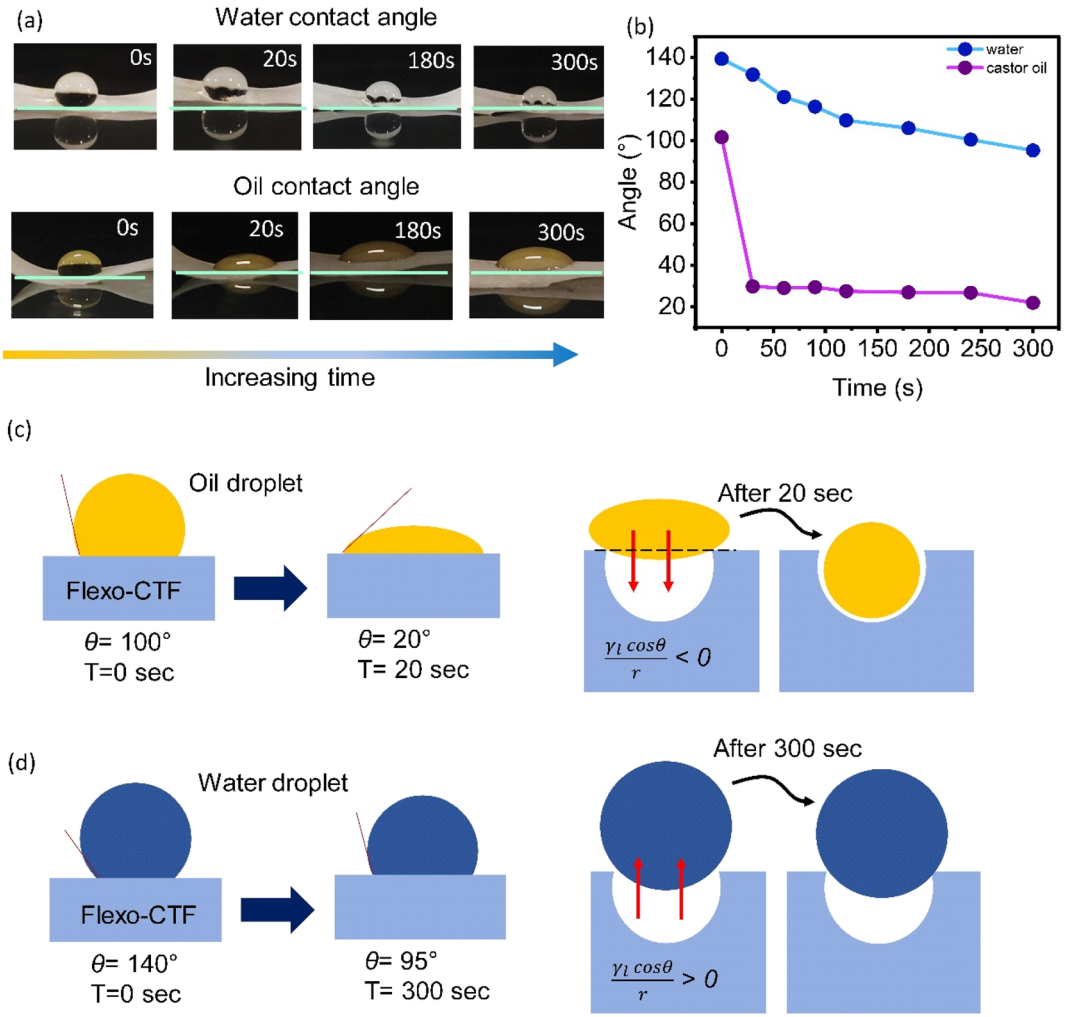

Fig. 3 (a) Optical images of the contact angle of water and oil on the Flexo-CTF surface at different time intervals. (b) Plot of the contact angle of water and oil with respect to time. (c) Schematic showing the mechanism of oleophilicity of the Flexo-CTF surface. (d) Schematic showing the mechanism of hydrophobicity of the Flexo-CTF surface.

~95° in 300 seconds. This implies that the film is hydrophobic and adsorbs/absorbs only negligible amounts of water. Similarly, it was observed that for the oil drop, the contact angle changed from ~102° to ~22° in 300 seconds, which implied that the film was oleophilic in nature. Due to the porous nature of the TPU-film, it prevents water adsorption into it.[53] The high viscosity of oil compared to water results in high sorption capacity and low capillary action into the porous surface. One benefit is that it can improve the adhesion of oil to the surface, thereby boosting sorption capacity. However, heavier oils can have their sorption capacity reduced, which prevents the oil from penetrating the core of the film sorbents. The intermolecular force that results when one fluid applies pressure to another's surface or liquid is called surface tension. Oil could permeate the sorbents and become trapped within the solid sorbent, as indicated by a low surface tension value. In this study, the four types of oils (castor oil, vegetable oil, pain relief oil and gasoline) selected for our investigation are typically utilized in daily life and production. The viscosity of castor oil is 311.5 mPa s, whereas the viscosity of gasoline is 0.5 mPa s, and the viscosity of other oils is between these values (Table S1†). The surface tension of castor oil is 0.01489 N m^{-1} and that of gasoline is 0.02504 N m^{-1}. Hence, the adsorption of liquids on the porous material is governed by the equation[54]

$$K_s = \rho \times \left(\frac{\sigma}{\mu}\right)^{\frac{1}{2}} \times \left(\frac{\varepsilon^*}{\tau}\right) \times r_0^{\frac{1}{2}} \times \left(\cos\frac{\theta}{2}\right)^{\frac{1}{2}} \quad (3)$$

where K_s is the suction coefficient, ρ is the density of the liquid, σ is the liquid surface tension, μ is the liquid viscosity, r_0 is the average pore radius, and ε^* is the effective suction porosity, τ is the average tortuosity factor, and θ is the contact angle. According to eqn (3), the contact angle and surface tension are directly proportional, while viscosity is inversely proportional. Therefore, as the surface tension decreases or the viscosity increases, the contact angle also decreases, which explains the high adsorption efficiency of oils on Flexo-CTF compared to petroleum.

Further, the superoleophilicity of the film was also explained by the intrusion pressure (ΔP) given by eqn (1). For oils, the surface tension is lower than that of water; hence, the intrusion

pressure decreases, which facilitates the oil to permeate into the pores of the film and remain adsorbed on the surface. Therefore, it is evident that while superoleophilicity and adsorption capacity are facilitated by the low surface tension of the oil solvents, the viscosity of the oil solvents significantly influences the variation in adsorption capacity among these oil sorbents. Therefore, it could be seen that the adsorption of the oil on the film increased with the increase in the viscosity and decrease in surface tension of the oil (Fig. 3c). Meanwhile, the intrusion pressure (ΔP) increases for water due to its higher surface tension. This prevents water from penetrating the film, resulting in low water adsorption on the film, and the surface becomes hydrophobic (Fig. 3d).[55]

3.4 Dye-adsorption using Flexo-CTF

Following the good adsorption quality of Flexo-CTF, an experiment was conducted to study the adsorption of dye molecules from contaminated water. It was observed that the efficiency of dye adsorption increased with time, as shown in Fig. 4a and b. The efficiency of adsorption was measured using the calorimetric absorbance (A_c) method. Digital photographs and the RGB values were used to analyze the different stages of adsorption. A regular smartphone camera was used to capture pictures in this experiment. Since this method is easy to use, quantification is straightforward, accurate and affordable; therefore, it was employed. Colorimetric detection quantifies color variations in RGB pixel intensity. The process involved capturing pictures of the different phases of adsorption and importing them to a software (ImageJ). Using the software, the required region of interest was selected, and its average RGB (I_{RGB}) and the average RGB value of the background (I_{BG}) were calculated.[56] Further, using eqn (2), the colorimetric absorbance was calculated, and the adsorption efficiency was measured using the following equation,

$$\text{Adsorbance efficiency } (\%) = \frac{A_0 - A}{A_0} \times 100 \quad (4)$$

where A_0 is the colorimetric absorbance value at $t = 0$ minutes and A is the colorimetric absorbance value at a particular time (t).

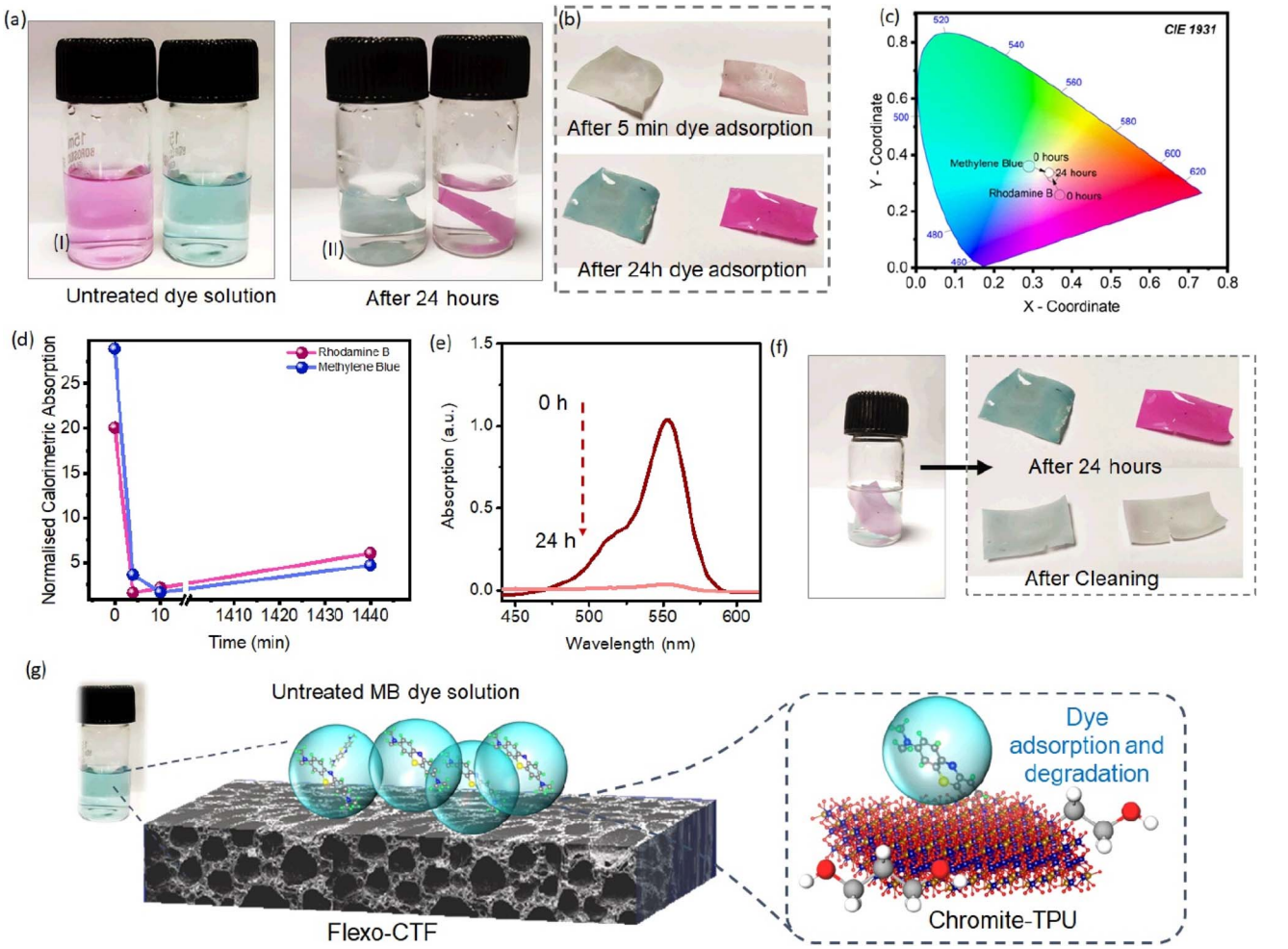

Fig. 4 (a) Optical image of the dye adsorption of MB and RhB for a time interval of 24 hours. (b) Optical image of the Flexo-CTF for the dye adsorption after 5 minutes and after 24 hours. (c) Chromaticity diagram showing variation in the RGB values of the solution from 0 to 24 hours. (d) Plot of normalised calorimetric adsorption *versus* time (e) UV vis plot of the dye adsorption from 0 to 24 hours. (f) Optical image of cleaning Flexo-CTF using acetone. (g) Schematic of the mechanism of interaction of the dye with the chromite nanosheets.

Fig. 4c shows the variation of color using colorimetric coordinates. The CIE colorimetric coordinates were calculated for both dyes as a function of time. It shows that after 24 hours of adsorption, the color coordinates were almost in the white region (average red-green blue (RGB) value was ~207 for MB and ~206 for RhB). Furthermore, we calculated the colorimetric absorbance values at various time intervals (0, 4, 10 minutes, and 24 hours), which are shown in Fig. 4d. The adsorption efficiency of Flexo-CTF was found to be ~84 ± 8% for MB dye and 70 ± 8% for RhB in 24 hours without any external stimuli. To validate the colorimetric methods for calculating efficiency, we have further used a spectroscopic technique, as shown in Fig. 4e. The adsorption efficiency was further measured, and it was found to be ~90 ± 3%. To study the reusability of the CTF, the adsorbed dye was cleaned by dipping the film in acetone solvent and sonicating in the bath sonicator for 5 minutes. This removed almost all the dye adsorbed on the Flexo-CTF, which made it possible to reuse it further (Fig. 4f). The surface chemistry, mainly surface charges and the presence of functional groups of Flexo-CTF, played an important role in adsorbing the dye as the porous surface increased the effective area, allowing more dye molecules to interact with the chromite nanosheets, as schematically shown in Fig. 4g.

The possible mechanism of dye adsorption (MB and RhB, cationic dyes) onto the CTF film involves the interactions (electrostatic, weak hydrogen bonding and π-interaction) between the charged surface of the atomically thin chromite and dye molecules. To confirm this, a zeta potential measurement was performed for the chromite 2D sheets and the plot is shown in Fig. S4.† It shows that the surface charge potential of the chromite sample was −32.4 mV, which indicates a negatively charged 2D layered surface. This negatively charged surface adsorbs the MB and RhB cationic dye molecules through electrostatic interactions and thus, the Flexo-CTF removes the toxic dye from the water bodies. The XPS plots (Fig. S5†) of 2D chromite show the different oxidation states (Fe^{3+}, Fe^{2+}, Cr^{3+} and Cr^{6+}) of the elements present. The deconvoluted O 1s spectrum further supports the formation of Fe–O and Cr–O bonds. Fe^{3+} and Cr^{6+} show high intensity peaks, suggesting the acidic surface and the existence of O^{-} or chromate groups. These anionic elements contribute to the observed zeta potential of −32.4 mV, consistent with a negatively charged surface. This negative charge facilitates the electrostatic attraction of cationic dyes. Furthermore, the presence of aromatic rings and functional groups is also responsible for the adsorption capacity, which is dependent on the surface chemistry. Surface charge and functional groups are among the most important properties for the adsorption of toxic dyes. To identify the functional groups on their surfaces, FTIR analysis was performed on Flexo-CTF before and after dye adsorption, as shown in Fig. S6.† There is a strong increase in the band intensity due to an increase in the adsorption of MB dye on the

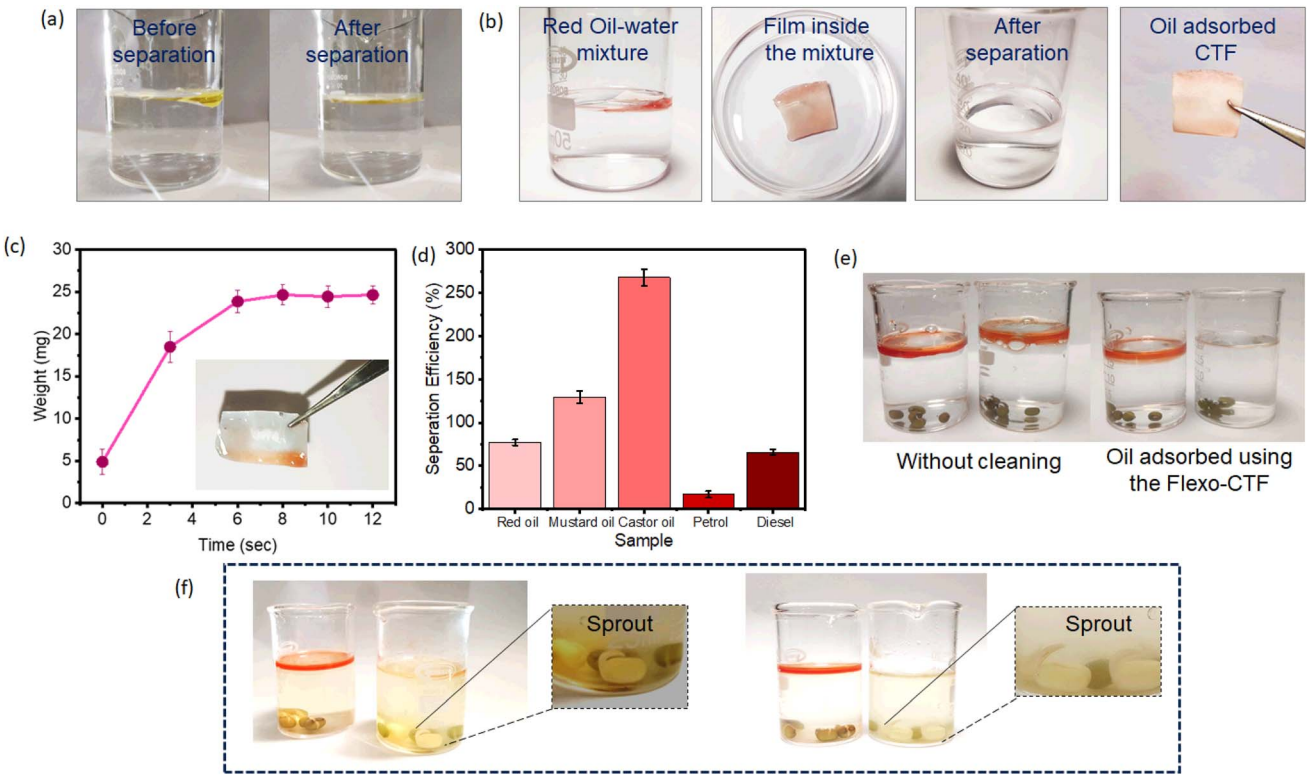

Fig. 5 (a) Optical images showing before and after the adsorption of mustard oil on Flexo-CTF. (b) Optical image showing the adsorption of red oil on the surface of Flexo-CTF and the film after adsorption. (c) Plot of the variation of the weight of the film after the adsorption of oil on the film. (d) Histogram plot showing the separation efficiency of the Flexo-CTF for different oils with the error analysis for a data set of $n = 5$. (e) Optical image showing the absorption of red oil using the Flexo-CTF containing the plant seeds. (f) Optical image showing difference in the germination of the seeds in the beaker cleaned using Flexo-CTF and the uncleaned beaker.

film. As the surface of the sample is enriched with a negative surface charge (zeta potential of −32.4 mV) and other functional groups (discussed earlier in Fig. 2c), it helps to form H-bonds with the nitrogen or oxygen atoms in the MB dye. Also, the molecular structure of the MB dye possesses a cation, which may lead to π-interaction with the Flexo-CTF film. Therefore, it was noted that the electrostatic interaction, hydrogen bond and π-interaction played a critical role in the adsorption of dyes.[57,58]

3.5 Oil adsorption from water using Flexo-CTF

After studying the adsorption properties of CTF by measuring its contact angle and using the film for dye adsorption, Flexo-CTF was further employed for oil–water separation. The Flexo-CTF adsorbed the oils on its surface due to its porous structure. The weight of the film before and after adsorption was noted, and the oil adsorption efficiency of the film was calculated using the following formula:

$$A\ (\%) = \frac{W_2 - W_1}{W_1} \times 100 \quad (5)$$

where W_1 is the weight of the film before adsorbing the oil and W_2 is the weight of the film after adsorbing the oil. The adsorption capacity was determined using eqn (4). The adsorption capacity of the film for castor oil was ∼268%, whereas for vegetable oil (Fig. 5a), it was ∼130%. For red oil (Fig. 5b), diesel and petrol, the adsorption capacities were ∼77%, ∼66% and ∼17%, respectively. A plot of the weight of the film with oil adsorbed *versus* time was plotted, and it was seen that the amount of oil adsorbed was saturated after a certain time (Fig. 5c). A plot of adsorption capacity *versus* different types of oil was plotted (Fig. 5d), and it was observed that the adsorption for castor oil was the highest and that for petrol was the lowest. The viscosity and surface tension of the oil solvents are responsible for the different adsorption capabilities of these oils. Further, to apply these properties in a real-life situation, two beakers were filled with normal water. The water in both beakers was polluted with the oils (as shown in Fig. 5e). The polluted water in one of the beakers was treated using Flexo-CTF by adsorbing the oil present in it. Additionally, some organic seeds were added to both beakers and the behavior of the seeds was observed for seven days. It was observed that the seeds in the polluted water started to germinate at a lower rate than those in the treated water, as seen in digital images (Fig. 5f). This successfully demonstrated that the film can be used in polluted water bodies to protect aquatic life from water pollution by adsorbing the oils.

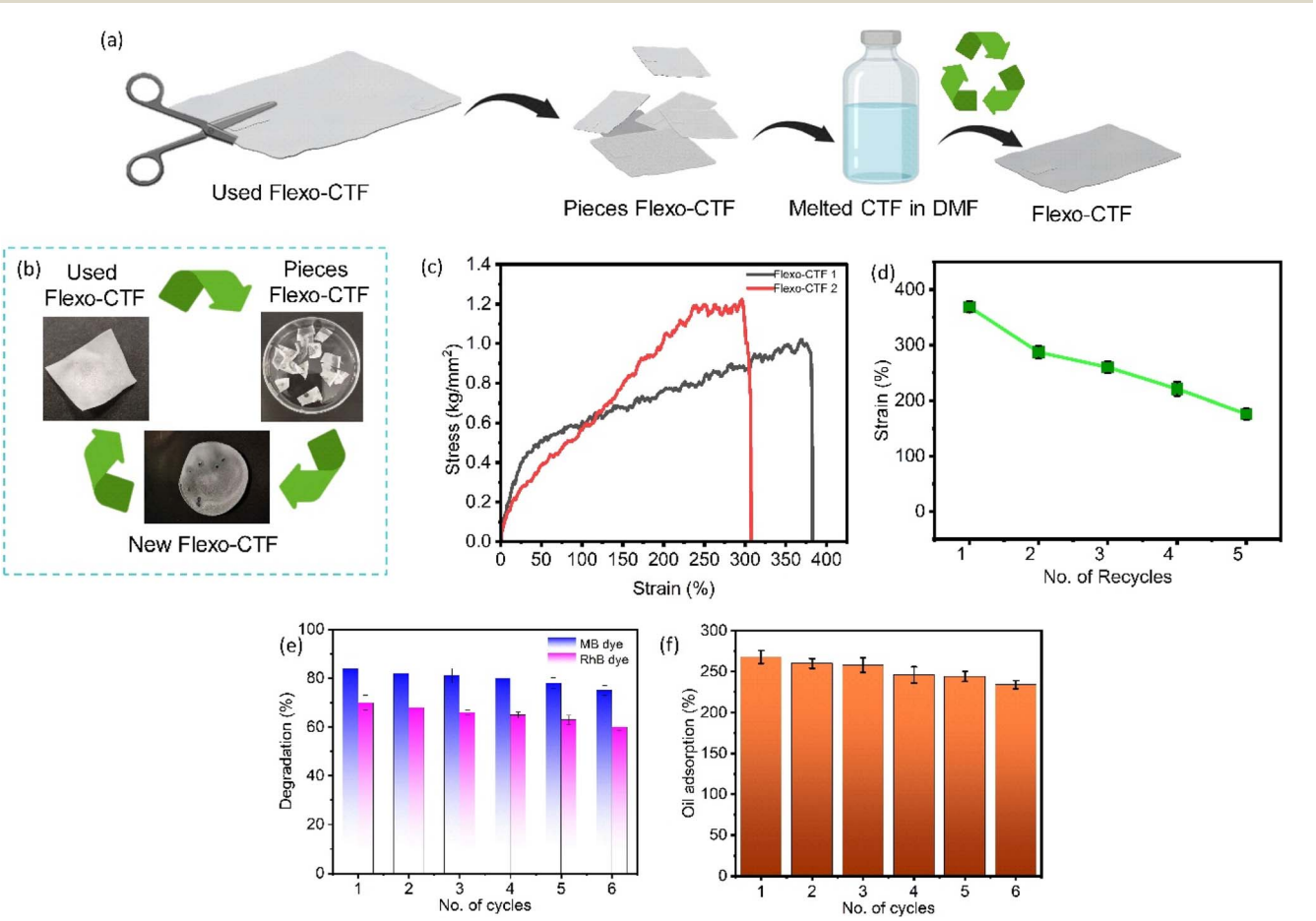

Fig. 6 (a) Schematic showing the process of recycling Flexo-CTF. (b) Optical image showing the recycling of the Flexo-CTF. (c) Stress *vs.* strain curve of Flexo-CTF after 2 times of re-synthesis. (d) Change in the strain of the film after 5 times of re-synthesis. (e) Histogram plot showing the dye adsorption for 6 cycles of recycling the film. (f) Histogram plot showing the oil adsorption for 6 cycles of recycling the film.

3.6 Recyclability of the Flexo-CTF

Interestingly, the Flexo-CTF was further successfully demonstrated to be recyclable, which is an important property for environmental sustainability. When the system is used for a long duration in harsh conditions, it is bound to wear and tear despite its remarkable mechanical properties. Therefore, rather than discarding the system, which might create more environmental pollution, it could be recycled. Here, the recycling process was done using a simple and efficient method, as schematically shown in Fig. 6a and b. Once the film is in an unusable condition, it is cleaned, dried, and cut into small pieces. These small pieces are then dissolved by adding DMF and heating the solution to ~70 °C, which causes the excess DMF to evaporate and form pores as used in the synthesis process of the initial film. The chromite-TPU solution is then left to dry for 8–12 hours. This new recycled film has similar mechanical and contact angle properties to the original film, as shown in Fig. 6c and S7.† The mechanical strain of the recycled film decreased by ~163% compared to the original film after it was resynthesized five times from used Flexo-CTF film (Fig. 6d). Further, the contact angle changed by less than ~1% after recycling the Flexo-CTF. This was further verified by performing dye adsorption experiments with both MB and RhB dyes using the recycled Flexo-CTF for several cycles. We observe a similar efficiency of dye adsorption to that of the initial film, as seen in Fig. 6e. Moreover, oil adsorption was also carried out using the recycled film for several cycles, and an almost consistent oil adsorption efficiency was observed for the recycled films (Fig. 6f).

The adsorption efficiency of Flexo-CTF is higher than that of any other reported materials, as shown in Table S2.† It is noted that there have been very few works on the recycling property of the oil–water separator. In this work, the recycling properties of the TPU-chromite film are novel and sustainable for the environment as the film can be recovered after multiple uses and reused as a new film. In addition, the cost of synthesizing Flexo-CTF is minimal as the individual cost of materials is very low, including natural oxides, which are abundantly available in nature as well as the TPU polymer, a low-cost material. The process of fabricating the film does not require excessive energy and it is a single-step chemical process. Hence, when considering the cost of all these factors and comparing with the materials that are already available and utilize expensive elements, such as titanium and molybdenum, the overall cost to synthesize Flex-CTF is minimal.

Finally, the superhydrophobic property of Flexo-CTF prompted the self-cleaning ability of the film (Fig. S8†). This was observed by sliding the soil with particles of different sizes. The larger particles slid through the film and the smaller particles became trapped on the film due to the porous structure of the film. Further, water was dropped on the film and due to its superhydrophobic property, the water removed all the smaller dust particles, demonstrating a remarkable self-cleaning property of the film.

4 Conclusions

In conclusion, we have successfully fabricated a superhydrophobic/oleophilic nanocomposite film using TPU as the matrix and the natural chromite nanosheets as the dispersed material. The film is used to adsorb oils and other toxic dyes from the surface of large water bodies. The hydrophobicity and oleophilicity of the Flexo-CTF were successfully explained using the contact angle and surface tension of water and oil on the film. Moreover, the adsorption efficiency of Flexo-CTF for castor oil was measured to be ~268% and it showed a dye adsorption efficiency of ~90% for the MB dye. Additionally, the Flexo-CTF film is recyclable from the old Flexo-CTFs for further use, which makes it sustainable. It demonstrated very good stability even after being recycled multiple times and showed similar mechanical and adsorption properties. Hence, this film can be used commercially to clean the surface of oceans and other huge water bodies.

Data availability

The data supporting this article have been included as part of the ESI.†

Author contributions

The manuscript was written through the contributions of all the authors. All the authors have given approval to the final version of the manuscript.

Conflicts of interest

The authors declare no competing financial interest.

Acknowledgements

P. K. and R. D. S. are thankful to the financial support from Science and Engineering Research Board (currently ANRF), India, for the sponsored project *via* SRG grant (SRG/2023/001763). All the authors thank Christ University for providing research facilities.

References

1 R. S. Sutar, S. S. Latthe, A. R. Jundle, P. P. Gaikwad, S. S. Ingole, S. Nagappan, Y. H. Kim, A. K. Bhosale, V. S. Saji and S. Liu, *Mar. Pollut. Bull.*, 2023, **198**, 115790.
2 M. Asiltürk and Ş. Şener, *Chem. Eng. J.*, 2012, **180**, 354–363.
3 I. K. Konstantinou and T. A. Albanis, *Appl. Catal., B*, 2004, **49**, 1–14.
4 S. Kordjazi, K. Kamyab and N. Hemmatinejad, *Adv. Compos. Hybrid Mater.*, 2020, **3**, 001508.
5 H. Gong, B. Yu, F. Dai and Y. Peng, *Colloids Surf., A*, 2018, **550**, 27–36.
6 J. Saththasivam, K. Loganathan and S. Sarp, *Chemosphere*, 2016, **144**, 671–680.
7 S. Gupta and N.-H. Tai, *J. Mater. Chem. A*, 2016, **4**, 1550–1565.
8 P. Sobolciak, A. Popelka, A. Tanvir, M. A. Al-Maadeed, S. Adham and I. Krupa, *Water*, 2020, **12**, 123419.
9 I. V. Maggay, Y. Chang, A. Venault, G. V. Dizon and C. J. Wu, *Sep. Purif. Technol.*, 2021, **259**, 117983.

10 C. Su, *Appl. Surf. Sci.*, 2010, **256**, 2122–2127.
11 Y. Li, X. J. Huang, S. H. Heo, C. C. Li, Y. K. Choi, W. P. Cai and S. O. Cho, *Langmuir*, 2007, **23**, 2169–2174.
12 W. Chen, A. Y. Fadeev, M. C. Hsieh, D. Öner, J. Youngblood and T. J. McCarthy, *Langmuir*, 1999, **15**, 3395–3399.
13 L. Feng, S. Li, Y. Li, H. Li, L. Zhang, J. Zhai, Y. Song, B. Liu, L. Jiang and D. Zhu, *Adv. Mater.*, 2002, **14**, 1857–1860.
14 T. Sun, L. Feng, X. Gao and L. Jiang, *Acc. Chem. Res.*, 2005, **38**, 644–652.
15 A. Marmur, *Langmuir*, 2004, **20**, 3517–3519.
16 C. Su, J. Li, H. Geng, Q. Wang and Q. Chen, *Appl. Surf. Sci.*, 2006, **253**, 2633–2636.
17 C.-T. Hsieh, J.-M. Chen, R.-R. Kuo, T.-S. Lin and C.-F. Wu, *Appl. Surf. Sci.*, 2005, **240**, 318–326.
18 A. Nakajima, K. Hashimoto and T. Watanabe, *Vienna*, Springer Vienna, 2001, pp. 31–41.
19 J. Wu, N. Wang, L. Wang, H. Dong, Y. Zhao and L. Jiang, *ACS Appl. Mater. Interfaces*, 2012, **6**, 3207–3212.
20 S. P. Dalawai, M. A. S. Aly, S. S. Latthe, R. Xing, R. S. Sutar, S. Nagappan, C. S. Ha, S. S. Sadasivuni and S. Liu, *Prog. Org. Coat.*, 2020, **138**, 105381.
21 H. Ji, R. Zhao, Y. Li, B. Sun, Y. Li, N. Zhang, J. Qiu, X. Li and C. Wang, *Colloids Surf., A*, 2018, **538**, 173–183.
22 C. W. Yao, S. Tang, D. Sebastian and R. Tadmor, *Appl. Surf. Sci.*, 2020, **504**, 144493.
23 F. Li, W. Kong, X. Zhao and Y. Pan, *ACS Appl. Mater. Interfaces*, 2020, **12**, 18074–18083.
24 N. M. Phan, J.-H. Kim, J. Kim, B. M. Weon and G.-R. Yi, *Appl. Surf. Sci.*, 2021, **570**, 151088.
25 S. S. Latthe, R. S. Sutar, T. B. Shinde, S. B. Pawar, T. M. Khot, A. K. Bhosale, K. K. Sadasivuni, R. Xing, L. Mao and S. Liu, *ACS Appl. Nano Mater.*, 2019, **2**, 799–805.
26 Z. He, H. Wu, Z. Shi, Z. Kong, S. Ma, Y. Sun and X. Liu, *ACS Omega*, 2022, **7**, 7084–7095.
27 H.-T. Ren, C.-C. Cai, W.-B. Cao, D.-S. Li, T.-T. Li, C.-W. Lou and J.-H. Lin, *ACS Appl. Nano Mater.*, 2023, **6**, 11925–11933.
28 E. Velayi and R. Norouzbeigi, *Surf. Coat. Technol.*, 2020, **385**, 125394.
29 Y. Guo, X. Zhou, X. Yi, D. Wang and Q. Xu, *Appl. Nanosci.*, 2020, **10**, 1511–1520.
30 M. Sajid, I. Ihsanullah, M. T. Khan and N. Baig, *Sep. Purif. Technol.*, 2023, **305**, 122453.
31 J. Li, Z. Zhao, Y. Zhang, M. Li, Z. Luo and L. Luo, *J. Sol-Gel Sci. Technol.*, 2017, **82**, 299–307.
32 O. Rius-Ayra, A. Biserova-Tahchieva, V. Sansa-López and N. Llorca-Isern, *Langmuir*, 2022, **38**, 5943–5953.
33 O. Rius-Ayra, A. Biserova-Tahchieva and N. Llorca-Isern, *Chemosphere*, 2023, **311**, 137148.
34 O. Rius-Ayra, A. Biserova-Tahchieva, V. Sansa-López and N. Llorca-Isern, *Prog. Org. Coat.*, 2022, **170**, 107009.
35 D. Lang, G. Liu, R. Wu, G. Chen, C. Zhang, C. Yang, W. Wang, J. Wang and J. Fu, *Chem. Eng. J.*, 2023, **471**, 144752.
36 J. Bannerjee and K. Dutta, *Polym. Compos.*, 2019, **40**, 4473–4488.
37 S. Sriram, R. K. Singh and A. Kumar, *Surf. Interfaces*, 2020, **19**, 100472.
38 Y. Li, H. Zhang, Y. Liu, H. Wang, Z. Huang, T. Peijs and E. Bilotti, *Composites, Part A*, 2018, **105**, 9–18.
39 D. Bokov, A. T. Jalil, S. Chupradit, W. Suksatan, M. J. Ansari, I. H. Shewael, G. H. Valiev and E. Kianfar, *Adv. Mater. Sci. Eng.*, 2021, 5102014.
40 J. C. Shearer, M. J. Fisher, D. Hoogeland and E. R. Fisher, *Appl. Surf. Sci.*, 2010, **256**, 2081–2091.
41 K. Li, M. Liang, M. Zhang, J. Nie and L. Bao, *Fibres Polym.*, 2024, **25**, 2443–2456.
42 T. Lee, S. H. Min, M. Gu, Y. K. Jung, W. Lee, J. U. Lee, D. G. Seong and B.-S. Kim, *Chem. Mater.*, 2015, **27**(11), 3785–3796.
43 T. P. Yadav, S. N. Shirodkar, N. Lertcumfu, S. Radhakrishnan, F. N. Sayed, K. D. Malviya, G. Costin, R. Vajtai, B. I. Yakobson, C. S. Tiwary and P. M. Ajayan, *Adv. Mater. Interfaces*, 2018, **5**, 1800549.
44 G. Yihao, C. Fangqin and P. Zihe, *Polymers*, 2019, **11**, 806.
45 P. L. Mahapatra, P. Kumbhakar, B. Lahiri, S. K. Sinha and C. S. Tiwary, *Mater. Res. Bull.*, 2022, **146**, 111590.
46 A. Taufiq, R. E. Saputro, S. Sunaryono, Y. A. Haiyanto, N. Hidayat, A. Hidayat, N. Mufti, H. Susanto and M. Mujamilah, *J. Phys.:Conf. Ser.*, 2018, **1093**, 012010.
47 D. Azarifar, Y. Abbasi, M. Jaymand, M. A. Zolfigol, M. Ghaemi and O. Badalkhani, *J. Organomet. Chem.*, 2019, **895**, 55–63.
48 D. Yuliantika, A. Taufiq, A. Hidayat, S. Sunaryono, N. Hidayat and S. Soontaranon, *IOP Conf. Ser.:Mater. Sci. Eng.*, 2019, **515**, 012047.
49 N. Millaty Abadiah, D. Yuliantika, Y. A. Hariyanto, R. E. Saputro, M. Masruroh, A. Taufiq and S. Soontaranoon, *Conf. Ser. Earth Environ. Sci.*, 2019, **276**, 012064.
50 A. Taufiq, N. Wahyuni, R. E. Saputro, N. Mufti, S. Sunaryono, A. Hidayat, D. Yuliantika, N. Hidayat and M. Mujamilah, *Mol. Cryst. Liq. Cryst.*, 2019, **694**, 1723897.
51 A. Taufiq, R. E. Saputro, S. Sunaryono, Y. A. Hariyanto, N. Hidayat, A. Hidayat, N. Mufti, H. Susanto and M. Mujamilah, *J. Phys.:Conf. Ser.*, 2019, **1093**, 012010.
52 V. P. Senthil, J. Gajendiran, S. G. Raj, T. Shanmugavel, K. G. Ramesh and P. C. Reddy, *Chem. Phys. Lett.*, 2018, **695**, 19–23.
53 S. Jasmee, G. Omar, N. Masripan, N. A. B., A. A. Kamarolzaman, A. S. Ashikin and F. C. Ani, *Mater. Res. Express*, 2018, **5**, 096304.
54 A. Escardino, V. Beltràn, A. Barba and E. Sànchez, *Br. Ceram. Trans.*, 1999, **98**(5), 225–229.
55 E. Zhang, Z. Cheng, T. Lv, Y. Qian and Y. Liu, *J. Mater. Chem. A*, 2015, **3**, 13411–13417.
56 T. Alawsi, G. P. Mattia, Z. Al-Bawi and R. Beraldi, *Sens. Biosensing. Res.*, 2021, **32**, 100404.
57 V.-P. Dinh, T.-D.-T. Huynh, H. M. Le, V.-D. Nguyen, V.-A. Dao, N. Q. Hung, L. A. Tuyen, S. Lee, J. Yi, T. D. Nguyen and L. V. Tan, *RSC Adv.*, 2019, **9**, 25847–25860.
58 J. Wang, Y. Tan, H. Yang, L. Zhan, G. Sun and L. Luo, *Sci. Rep.*, 2023, **13**, 21174.